Pediatr Radiol (2007) 37:549–555
DOI 10.1007/s00247-007-0461-x

ORIGINAL ARTICLE

Pilomatricomas in children: imaging characteristics with pathologic correlation

Hyun Wook Lim · Soo Ah Im · Gye-Yeon Lim · Hyun Jin Park · Heejeong Lee · Mi Sook Sung · Bong Joo Kang · Jee Young Kim

Received: 21 April 2006 / Revised: 26 February 2007 / Accepted: 14 March 2007 / Published online: 17 April 2007

Abstract
Background Although pilomatricoma commonly occurs in children, there is still a poor understanding of the imaging characteristics of pilomatricoma and lack of agreement regarding its imaging findings and histopathologic features.
Objectives To characterize the radiologic appearance of pilomatricomas on US, CT, and MR and to correlate the imaging findings with histopathologic features.
Materials and methods The imaging findings of 47 pilomatricomas on US (n=17), CT (n=31), and MR (n=5) were retrospectively evaluated. Pathologic specimens of all cases were reviewed and compared with imaging findings.
Results All lesions were well-circumscribed, subcutaneous nodules with partial attachment to the overlying skin. On US, the lesions were mostly hyperechoic with posterior acoustic shadowing and hypoechoic rim. On CT, they appeared as enhancing soft-tissue masses with varying amounts of calcification. MR findings were internal reticulations and patchy areas on T2-weighted images and contrast-enhanced T1-weighted images, corresponding to edematous stroma on pathology. Peritumoral inflammatory changes and connective capsule on pathology were well correlated with imaging findings.
Conclusion Pilomatricoma should be considered when US or CT shows a well-defined hyperechoic or calcific nodule in subcutaneous fat attached to the skin in children. MR images may be helpful in diagnosis. Pathologic findings are well correlated with imaging findings.

Keywords Pilomatricoma · US · CT · MRI · Children

H. W. Lim · S. A. Im (✉) · G.-Y. Lim · H. J. Park · H. Lee · M. S. Sung · B. J. Kang · J. Y. Kim
Department of Radiology, Kangnam St. Mary's Hospital, The Catholic University of Korea,
505 Banpo-dong, Seocho-gu,
Seoul 137-701, South Korea
e-mail: saim@catholic.ac.kr

Introduction

Pilomatricoma, also known as calcifying epithelioma of Malherbe, is a benign subcutaneous tumor that arises from hair cortex cells [1–3]. Pilomatricoma commonly occurs in children and most frequently appears in the head and neck region [4]. Although pilomatricoma is the most commonly excised superficial mass in children after epidermoid cyst and lymph nodes, it is frequently misdiagnosed and not usually considered in the clinical differential diagnosis [5, 6]. In addition, there is still only a poor understanding of the imaging characteristics of pilomatricoma and there is lack of agreement regarding its imaging findings and histopathologic features [6].

Histologically, pilomatricoma is a sharply demarcated tumor consisting of irregular islands of epithelial cells embedded in rather cellular stroma and situated in the dermis or subcutaneous fat layer. Epithelial cells with basophilic cytoplasm are seen at the periphery of these tumors, arranged in an arc-like fashion. Basaloid cells are transformed into shadow cells, also known as "ghost" cells, which are more centrally located. These cells have lost their nuclei and are filled with keratin and stain eosinophilic. The transitional cells, which are localized between the basaloid and shadow cells, are thought to represent apoptotic cells that are finally becoming shadow cells [6]. The stroma is collagenous and contains dilated blood vessels. Chronic inflammation with foreign body reaction can be seen in the stroma adjacent to the shadow cells [7]. Calcium deposition

commonly occurs in the shadow cell region and stroma, with an incidence ranging from 69% to 85% [4, 8].

The purpose of this study is to characterize the radiologic appearance on US, CT, and MR of pilomatricomas and to correlate the imaging findings with the pathologic features.

Materials and methods

We retrospectively reviewed the US, CT, and MR findings of 47 pathologically confirmed pilomatricomas in 41 consecutive patients under 15 years of age. These patients were selected during an 8-year period (1997–2005). The cases were collected from multiple centers and were identified by reviewing pathology databases.

The study population included 16 boys and 25 girls with a mean age of 7.7 years (range 1–15 years). The lesions were prospectively diagnosed as pilomatricomas in 41% on clinical findings alone and in 83% by the original imaging reports (US 82%, CT 87%, MR 60%). All masses were surgically removed and pathologically proven. This study was performed in accordance with the regulations of the local institutional review board, and all patients gave written consent for the use of their information.

A total of 64 radiologic examinations were reviewed (11 radiography, 17 US, 31 CT, and 5 MR; both US and CT scans were performed on five patients). Radiography was performed in 11 lesions. US was performed in 14 patients (17 lesions) using either a 7-MHz linear transducer or a 5–12-MHz linear transducer (HDI 5000 or HDI 3000; ATL, Bothell, Wash.). CT was performed in 27 patients (31 lesions) with either a helical CT scanner (Somatom Plus-4; Siemens, Erlangen, Germany) or a 4-MDCT scanner (Somatom Volume Zoom; Siemens). Both unenhanced and enhanced CT scans were obtained in 23 patients (27 lesions). Only unenhanced or enhanced CT scans were obtained in two patients.

Five patients underwent MRI. MRI was performed using 1.5-T scanners (Signa, GE Medical Systems, Milwaukee, Wis.; Magnetom Vision Plus, Siemens, Erlangen, Germany; Gyroscan Intera, Philips Medical Systems, Best, The Netherlands). Spin-echo T1-weighted (T1-W) (TR/TE 500–560/13–18 ms), fast spin-echo T2-W (TR/TE 3,215–4,220/82–100 ms) images, and gadolinium-enhanced T1-W images (TR/TE 500–560/13–18 ms) were available in all patients. In addition, the field of view was 140–180 mm, the matrix number 224–256×192–256, the intersection gap 1.0–1.5 mm, and the section thickness 3.0–4.0 mm. Axial, coronal, and sagittal images were obtained using the above sequences. Three patients were imaged using a fat-suppressed T2-W fast spin-echo sequence. The fat-suppression technique used in T2-W fast spin-echo imaging and in contrast-enhanced T1-W spin-echo imaging was based on a frequency-selective excitation. Contrast-enhanced T1-W spin-echo imaging was performed after administration of 0.1 mmol/kg body weight of gadopentetate dimeglumine (Magnevist, Schering, Berlin, Germany).

The images were reviewed and consensus was reached by two pediatric radiologists (H.W.L., S.A.I.). The images were evaluated for the following characteristics: shape (round, oval, or lobular); size (maximal diameter); location; margin (well-defined or ill-defined); US echogenicity; CT attenuation; MR signal intensity (SI) (compared with the adjacent skeletal muscle); and the degree and pattern of enhancement on CT and MR. The lesions were also evaluated for the presence of calcification on CT and an internal anechoic or fluid-density area on US or CT. Surrounding subcutaneous changes (hyperechogenicity in the surrounding subcutaneous fat on US, peritumoral strandings in the surrounding subcutaneous fat on CT and MR images) were also evaluated.

On pathologic specimens, we evaluated calcification, the connective tissue capsule, peritumoral subcutaneous fat tissue and the tumor matrix. Correlation of the imaging findings and histopathologic features was carried out in all cases.

Results

The lesions were located in the subcutaneous fat layer of the head (49%), neck (28%), extremity (19%), and trunk (4%) (Table 1). Among the 41 study patients, two lesions were found in 6 patients (14%), among whom 3 had two lesions in the same anatomic region. With regard to lesion shape, 43 were oval, 3 were round, and 1 was lobular. The maximal diameter of the lesions ranged from 0.5 to 2.8 cm (mean 1.6 cm).

Table 1 Locations of pilomatricomas

Location	No. (%) of lesions
Head	23 (49)
Periauricular region	11
Cheek	4
Eyelid	4
Malar region	2
Orbital region	1
Forehead	1
Neck	13 (28)
Extremity	9 (19)
Upper extremity	8
Lower extremity	1
Trunk	2 (4)

Specimens of all lesions obtained by curettage or excision were available for pathologic review. The margins of all 47 lesions were well defined and partially attached to the overlying skin, and 20 lesions abutted the underlying muscles, 6 the parotid gland and 1 the pericranium on imaging. However, none of these lesions invaded the underlying muscles on pathology.

Various amounts of calcium deposition were present in all 47 lesions on pathologic review. Seven lesions with calcium deposition of more than 90% of the tumor showed bone metaplasia; these lesions had no basaloid cells. A connective tissue capsule was present in 37 lesions on pathology (79%). Chronic inflammation with a foreign body reaction of the stroma and peritumoral subcutaneous fat tissue was identified in 43 and 30 lesions (91% and 64%) on pathology, respectively. Foreign body-type giant cells, lymphocytes, and histiocytes were identified in the inflammatory area.

Radiography was performed in 11 lesions, identifying calcifications in 6 (55%). The patterns of calcifications were complete nodular (three lesions), diffuse amorphous (one lesion), peripheral rim-like (one lesion) and peripheral nodular (one lesion). The US findings are shown in Table 2. Of 17 lesions in 14 patients who underwent US, there were 15 heterogeneously hyperechoic lesions (88%) and 2 heterogeneously isoechoic lesions (12%). Posterior acoustic shadowing was seen in 15 lesions (88%). A peripheral hypoechoic rim was seen in 11 lesions (65%). Peritumoral hyperechogenicity was seen in 8 of 17 lesions (47%) (Fig. 1). An internal anechoic area was identified in two lesions on US and they showed posterior acoustic enhancement (Fig. 2). Color Doppler US was performed in 13 lesions and Doppler flow signals were observed in both the central and peripheral regions of two lesions (15%) and in the peripheral region of only four lesions (31%).

In 31 lesions evaluated by CT, all lesions were isodense relative to adjacent skeletal muscle on scans before contrast agent administration (Figs. 2, 3) and they showed mild to moderate enhancement on contrast-enhanced CT scans (Figs. 2, 3). Of the 31 lesions evaluated by CT, 25 (81%) had calcific foci within the mass, 18 had micro- or partial calcifications, 7 were completely calcified (Fig. 3), 10 (32%) showed peritumoral streaky densities, and 2 showed an area of fluid density (Fig. 2).

Table 2 US findings of pilomatricomas

US findings	No. (%) of lesions
Internal echogenicity	
Hyperechoic	15 (88)
Isoechoic	2 (12)
Hypoechoic rim	11 (65)
Peritumoral hyperechogenicity	8 (47)
Posterior acoustic shadowing	15 (88)
Posterior acoustic enhancement	2 (12)
Internal anechoic area	2 (12)

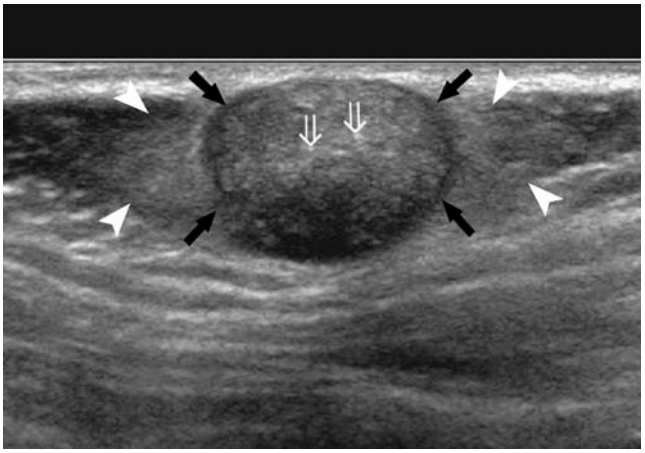

Fig. 1 An 8-year-old boy with pilomatricoma. The sonogram shows a well-defined, hyperechoic mass in the posterior neck. The lesion has a hypoechoic rim (*arrows*), tiny echogenic spots (*open arrows*), and peritumoral hyperechogenicity (*arrowheads*) in the surrounding subcutaneous fat tissue

On MR, the lesions were isointense in all five patients compared with adjacent skeletal muscle on T1-W images (Fig. 4). On T2-W images, all lesions were also isointense but showed internal hyperintense reticulations and patchy areas of increased SI (Figs. 4, 5). Peritumoral strandings in the surrounding subcutaneous fat were seen in three lesions (Fig. 5). In all masses evaluated by gadolinium-enhanced T1-W imaging, there was rim and internal reticular and patchy enhancement (Figs. 4, 5).

The imaging features in relation to the pathologic findings in the pilomatricomas of our series are shown in Table 3.

US showed posterior acoustic shadowing in 88% (15/17) and CT showed calcifications in 81% (25/31) of the lesions although various amounts of calcium deposition were present in the pathologic specimens of all lesions. An internal anechoic area on US images and an area of fluid density on CT images were correlated with an area of cystic degeneration histologically (Fig. 2). A hypoechoic rim on US and rim enhancement on contrast-enhanced T1-W MR images were correlated with a connective tissue capsule on pathology and were identified in 76% (10 /13) and 100% (5/5) of the lesions with a connective tissue capsule on pathology. Peritumoral hyperechogenicity on US and peritumoral strands on MR were well correlated with peritumoral inflammatory change on pathology, whereas only 53% (10/19) of the lesions with peritumoral change seen on pathology showed peritumoral strands on CT.

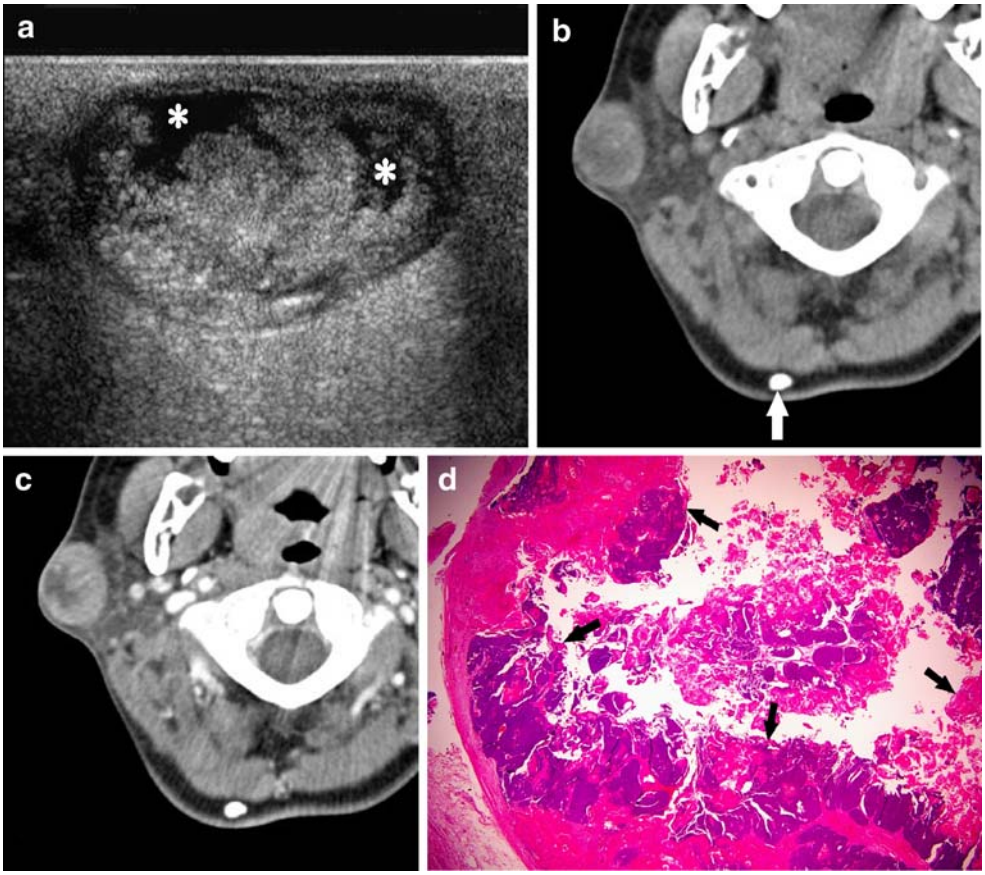

Fig. 2 A 9-year-old girl with pilomatricoma with cystic degeneration. **a** The sonogram shows a well-defined, complex echoic mass with posterior acoustic enhancement in the right infra-auricular region. The lesion has irregular anechoic areas (*asterisks*) corresponding to cystic degeneration on pathology. **b** Axial CT scan before contrast agent administration shows a well-marginated, heterogeneous density solid mass abutting the skin layer and parotid gland. Small nodular calcifications are seen in the mass. Another completely calcified pilomatricoma (*arrow*) is seen in the posterior neck. **c** Axial CT scan after contrast agent administration shows a well-enhanced mass with an irregular central poorly enhancing area. **d** Scanning view of the pathologic specimen shows cystic degeneration (*arrows*) of the pilomatricoma (H&E, ×12)

Four pilomatricomas showed varying amounts of peripheral nucleated basaloid cells on MR images, which were arranged in an arc-like fashion under the capsule of the compressed fibrous tissue. The fifth pilomatricoma imaged with MR had a paucity of basaloid cells; however, the lesion did not show any different SI on MR imaging compared with the other four lesions. In all five lesions, the intercellular stroma contained inflammatory and foreign-body-type giant cells (Fig. 5). Internal reticulations and patchy areas on the T2-W images corresponded to edematous stroma from which basaloid cells were absent (Fig. 5).

One lesion showed prominent bullous edematous thickening of the skin overlying the pilomatricoma on MR images, manifested as a low-SI area on T1-W images and as a hyperintense area on T2-W images (Fig. 4). Histologic examination of the bullous lesion revealed an edematous dermis with lymphatic vascular dilatation and markedly attenuated collagen bundles (Fig. 4).

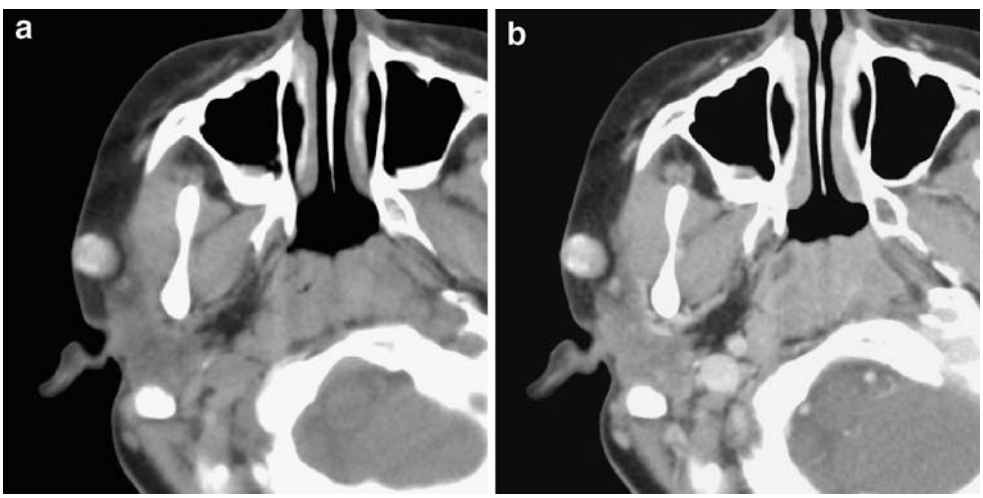

Fig. 3 An 11-year-old girl with pilomatricoma. **a**, **b** Axial CT scans before and after contrast agent administration show a well-demarcated, subtly enhancing soft-tissue mass in the subcutaneous fat partially abutting the overlying skin. Coarse calcifications are scattered in the mass

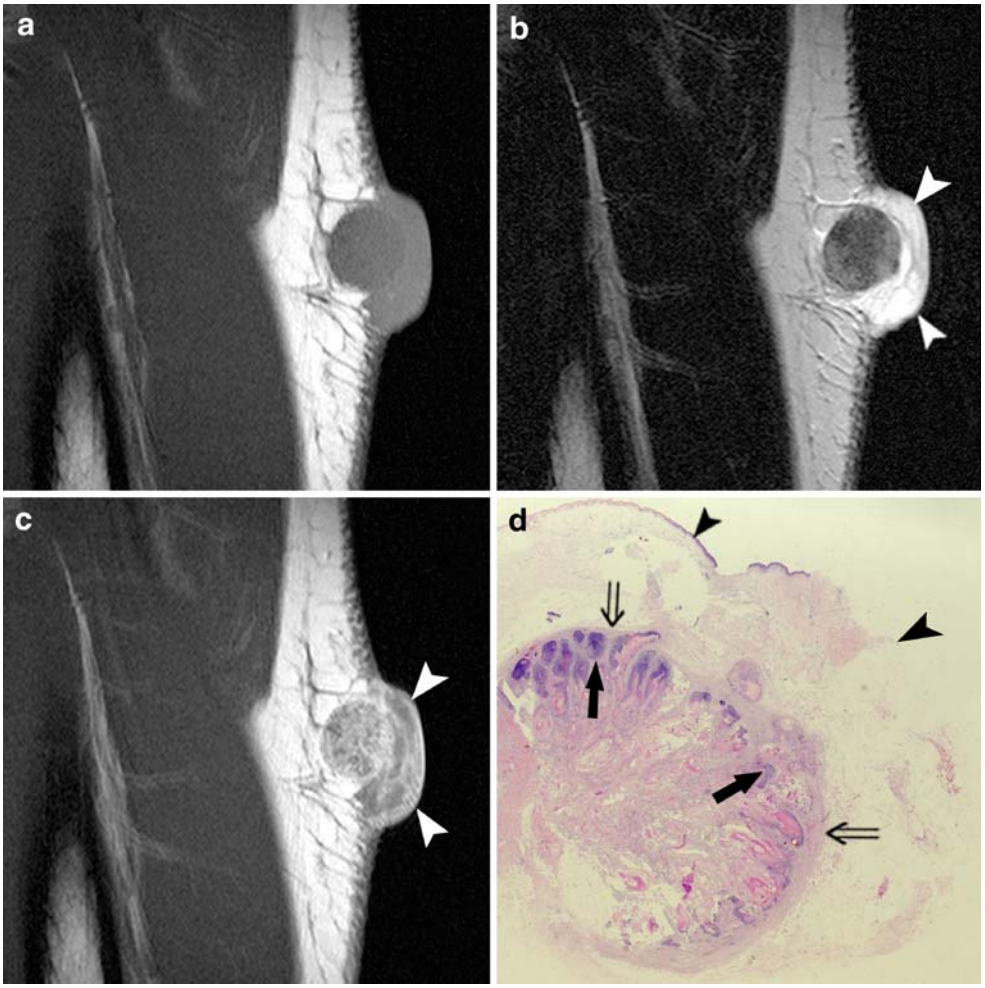

Fig. 4 A 9-year-old-boy with secondary anetoderma overlying pilomatricoma. **a** Coronal T1-W MR image (TR/TE, 500/18 ms) shows a well-demarcated, low-SI subcutaneous nodule with surrounding low SI. **b** Coronal T2-W MR image (TR/TE, 4,148/100 ms) shows patchy areas of increased signal in the periphery. Peritumoral dermal edema (*arrowheads*) appears as a higher signal in the overlying skin. **c** Contrast-enhanced T1-W MR image (TR/TE, 500/18 ms) shows diffuse reticular enhancement of the mass. The peritumoral dermal edema (*arrowheads*) is not enhanced except for enhancing septa-like structures. **d** Scanning view of the pathologic specimen shows nucleated basaloid cells (*arrows*) at the periphery, arranged in an arc-like fashion, under a capsule of compressed fibrous tissue (*open arrows*) and edematous dermis (*arrowheads*) (H&E, ×40)

Discussion

Pilomatricoma is an uncommon benign skin neoplasm originating from pluripotential cells that normally differentiate toward hair cortex cells [1, 2]. It was first described by Malherbe as a calcified tumor originating from the sebaceous gland and was referred to as "calcifying epithelioma of Malherbe" in 1880 [1]. It was renamed "pilomatrixoma" by Forbis and Helwig in 1961 [3]. Now, it is referred to as pilomatricoma rather than pilomatrixoma because the former is etymologically more reasonable [6].

Since pilomatricomas are superficially situated and typically present as subcutaneous or dermal nodules, surgical excision is directly performed without preoperative imaging. Therefore, in only a few reports of pilomatricoma are US, CT, or MR findings described [9, 10–17]. However, previous reviews have shown that the accuracy of preoperative diagnosis of pilomatricoma is less than 49% clinically [4, 8]. Hwang et al. [12] asserted recently that 33% of pilomatricomas are correctly diagnosed preoperatively on the basis of clinical findings alone and 76% by US. In our series, the 41% of the lesions were prospectively diagnosed as pilomatricomas on the basis of clinical findings alone and 83% by the original imaging reports (US 82%, CT 87%, MR 60%).

On US, pilomatricoma has been described as a well-defined, hyperechoic, or isoechoic nodule with a hypoechoic rim and posterior acoustic shadowing [10–12]. Hughes et al. [10] consider that the hypoechoic rim corresponds to the connective tissue capsule. The posterior acoustic shadowing is considered to represent calcifications [10]. On CT, pilomatricoma has been described as a well-defined mass of soft-tissue density with varying amounts of calcification and variable enhancement [13, 14]. In our study, 88% and 81% of lesions with calcium deposition microscopically showed posterior acoustic shadowing on US and calcification on CT, respectively. The connective tissue capsule identified on pathology appeared as a hypoechoic rim on US images in 73% of lesions in our series.

The US and CT findings in pilomatricoma in our series seem to correspond with those reported previously except for the findings of cystic degeneration and peritumoral changes. In two lesions in our series, there was cystic tumor

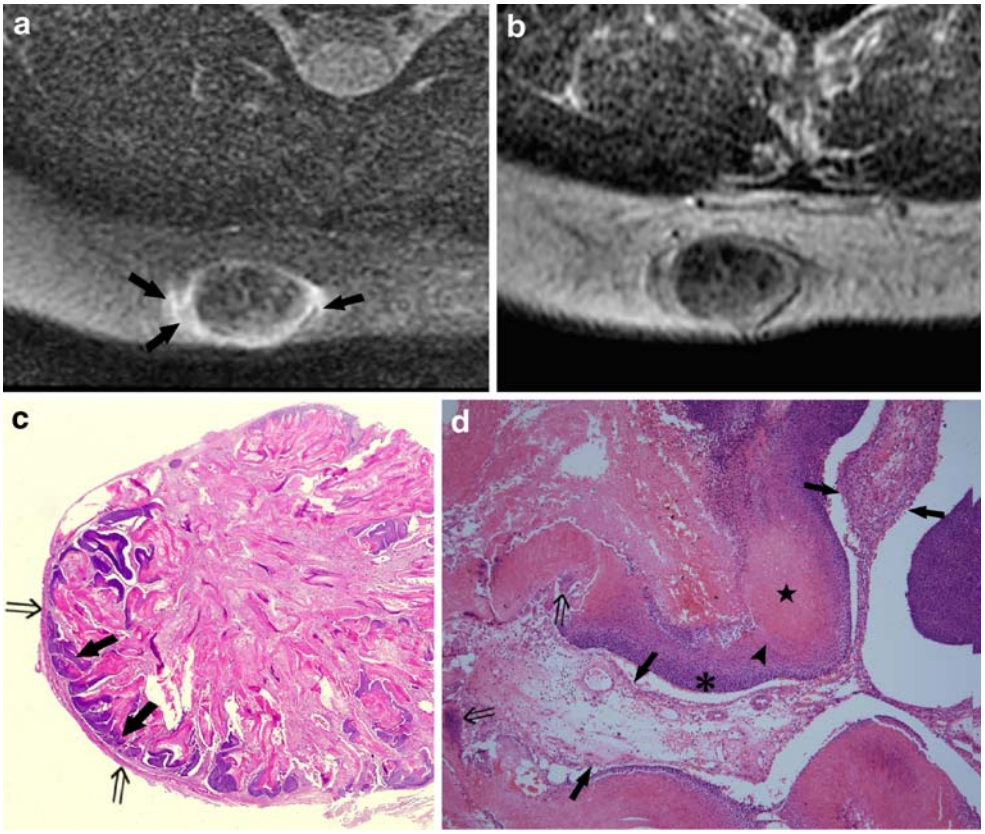

Fig. 5 An 11-year-old boy with pilomatricoma. **a** Axial fat-suppressed, T2-W MR image (TR/TE, 2,000/90 ms) shows a well-demarcated, low-SI subcutaneous nodule with internal reticular and peripherally increased SI. Peritumoral strands (*arrows*) are shown. **b** Gadolinium-enhanced, axial T1-W MR image (TR/TE, 400/15 ms) reveals diffuse reticular and rim enhancement. **c** Scanning view of a pathologic specimen shows a connective tissue capsule (*open arrows*) and islands of epithelial cells (*black arrows*) (H&E, ×40). **d** Microscopic view shows enucleated shadow cells (*star*) in the center and nucleated basophilic cells (*asterisk*) on the periphery of the mass and reveals the transition (*arrowhead*) from basaloid cells to shadow cells. Intercellular stroma with foreign body type giant cells (*open arrows*) and lymphocytes are also apparent (H&E, ×100)

degeneration appearing as an anechoic area with posterior acoustic enhancement on US and fluid density without enhancement on CT. This is the first imaging report of pilomatricoma with cystic degeneration. Reviewing the literature, we found no reports of pilomatricoma with cystic degeneration on US or CT, although tumor necrosis is often present in pilomatrix carcinoma [18].

On MR, pilomatricoma has been described as showing a homogeneous intermediate SI on T1-W images and inhomogeneous intermediate SI on T2-W images [15–17]. Hoffmann et al. [17] described a pilomatricoma with higher signal bands radiating from the center of the lesion to a higher signal periphery on a T2-W image. The periphery of the lesion enhanced with contrast agent, but the center did not. Hoffmann et al. suggested that the internal reticulations noted on T2-W and contrast-enhanced T1-W images represent basaloid cells. Masih et al. [9] described a pilomatricoma with internal reticulation and septations that were equally well seen on T2-W and gadolinium-enhanced fat-saturated images, possibly due to the presence of surrounding edematous stroma rather than basaloid cells, as the basaloid cells were sheets of avascular epithelial cells. Our findings support those of Masih et al. because the internal reticular and patchy areas on T2-W and contrast-enhanced T1-W images corresponded to the distribution of the intercellular stroma on pathologic specimens.

Some pilomatricomas are accompanied by chronic inflammation with a foreign body reaction with multinu-

Table 3 Imaging features and pathologic findings of pilomatricomas (*ND* not determinable)

Pathology (n=47)		US (n=17)		CT (n=31)		MR (n=5)	
Finding	No. (%) of lesions	Feature	No. (%) of lesions	Feature	No. (%) of lesions	Feature	No. (%) of lesions
Calcium deposition	47 (100)	Posterior acoustic shadowing	15 (88)	Calcifications	25 (81)	ND	–
Connective tissue capsule	37 (79)	Hypoechoic rim	11 (65)	ND	–	Rim enhancement	5 (100)
Peritumoral inflammatory change	30 (64)	Peritumoral hyperechogenicity	8 (47)	Peritumoral strands	10 (32)	Peritumoral strands	3 (60)

cleated giant cells and lymphocytes, and occasionally polymorphonuclear leukocytes in the surrounding subcutaneous fat tissue, probably due to mechanical stimulation [19]. These changes were correlated with peritumoral hyperechogenicity on US and with peritumoral strands on CT and MR images in our series. In our series, peritumoral changes were present in 47% of lesions on US, 32% on CT, 60% on MR, and 64% on pathology.

In our series, secondary anetoderma over pilomatricoma had developed in one patient. Anetoderma is clinically bulla-like or keloid-like in appearance and is characterized pathologically by dermal atrophy and edema, mononuclear cell infiltration, and lymphatic vascular dilatation [19, 20]. Secondary anetodermas are known to develop in various skin infections, inflammatory disorders, and tumors, but the association with pilomatricoma is very rare [19]. Moulin et al. [21] first described anetodermic cutaneous changes in the skin overlying a pilomatricoma in 1978. Although the etiology of secondary anetoderma is uncertain, continuous pressure and mechanical irritation are thought to be the major causes [20].

Radiologic differential diagnosis of pilomatricomas includes calcified lymph node, ossifying hematoma, hemangioma with phlebolith, granuloma annulare, and dermatofibrosarcoma. Anechoic vascular channels of hemangioma on US and the tendency of dermatofibrosarcoma protuberans to be unmineralized may be helpful in differential diagnosis [22]. Granuloma annulare is a soft-tissue mass without calcification and MR images show a mass with relatively decreased SI on all pulse sequences and extensive diffuse enhancement following gadolinium administration, whereas pilomatricomas tend to have calcification and show reticular and septal enhancement on MR images [23, 24].

Conclusion

Pilomatricoma should be considered in the differential diagnosis when a well-defined mass with various amounts of calcification is seen in the subcutaneous fat layer in children on US and CT. Pilomatricoma has characteristic MR findings with internal reticulations and patchy areas on T2-W and contrast-enhanced T1-W images, corresponding to distribution of edematous stroma on pathology. Rarely, intratumoral cystic degeneration or secondary anetodermic change may be associated with these lesions. Peritumoral inflammatory changes and connective capsule on pathology were well correlated with imaging findings.

Acknowledgements We thank Bonnie Hami, MA, Department of Radiology, University Hospitals Health System, Cleveland, Ohio, for her editorial assistance in preparing the manuscript.

References

1. Malherbe A, Chenantais J (1880) Note sur l'epitheliome calcifie des glandes sebacees. Prog Med 8:826–828
2. Kaddu S, Soyer HP, Cerroni L et al (1994) Clinical and histopathologic spectrum of pilomatricomas in adults. Int J Dermatol 33:705–708
3. Forbis R Jr, Helwig EB (1961) Pilomatrixoma (calcifying epithelioma). Arch Dermatol 83:606–618
4. Moehlenbeck FW (1973) Pilomatrixoma (calcifying epithelioma): a statistical study. Arch Dermatol 108:532–534
5. Knight PJ, Reiner CB (1983) Superficial lumps in children: what, when, and why? Pediatrics 72:147–153
6. Lan MY, Lan MC, Ho CY et al (2003) Pilomatricoma of the head and neck: a retrospective review of 179 cases. Arch Otolaryngol Head Neck Surg 129:1327–1330
7. Pirouzmanesh A, Reinisch JF, Gonzalez-Gomez I et al (2003) Pilomatrixoma: a review of 346 cases. Plast Reconstr Surg 112:1784–1789
8. Yencha MW (2001) Head and neck pilomatricoma in the pediatric age group: a retrospective study and literature review. Int J Pediatr Otorhinolaryngol 57:123–128
9. Masih S, Sorenson SM, Gentili A et al (2000) Atypical adult non-calcified pilomatricoma. Skeletal Radiol 29:54–56
10. Hughes J, Lam A, Rogers M (1999) Use of ultrasonography in the diagnosis of childhood pilomatrixoma. Pediatr Dermatol 16:341–344
11. Ulrich J, Wesarg I (2001) High-frequency ultrasound in the diagnosis of pilomatrixoma. Pediatr Dermatol 18:163
12. Hwang JY, Lee SW, Lee SM (2005) The common ultrasonographic features of pilomatricoma. J Ultrasound Med 24:1397–1402
13. Som PM, Shugar JM, Silvers AR (1998) CT of pilomatrixoma in the cheek. AJNR 19:1219–1220
14. Lee KH, Kim HJ, Suh CH (2000) Pilomatricoma in the head and neck: CT findings in three patients. J Comput Assist Tomogr 24:332–335
15. De Beuckeleer LH, De Schepper AM, Neetens I (1996) Magnetic resonance imaging of pilomatricoma. Eur Radiol 6:72–75
16. Ichikawa T, Nakajima Y, Fujimoto H et al (1997) Giant calcifying epithelioma of Malherbe (pilomatrixoma): imaging features. Skeletal Radiol 26:602–605
17. Hoffmann V, Roeren T, Moller P et al (1998) MR imaging of a pilomatrixoma. Pediatr Radiol 28:272
18. Sassmannshausen J, Chaffins M (2001) Pilomatrix carcinoma: a report of a case arising from a previously excised pilomatrixoma and a review of the literature. J Am Acad Dermatol 44:358–361
19. Fujioka M, Gozo N, Osamu M et al (2003) Secondary anetoderma overlying pilomatrixomas. Dermatology 207:316–318
20. Shames BS, Nassif A, Bailey CS et al (1994) Secondary anetoderma involving a pilomatricoma. Am J Dermatopathol 16:557–560
21. Moulin G, Bouchet B, Dos Santos G (1978) Anetodermic cutaneous changes above Malherbe's tumors. Ann Dermatol Venereol 105:43–47
22. Kransdorf MJ, Meis-Kindblom JM (1994) Dermatofibrosarcoma protuberans: radiologic appearance. AJR 163:391–394
23. Kransdorf MJ, Murphery MD, Temple HT (1998) Subcutaneous granuloma annulare: radiologic appearance. Skeletal Radiol 27:266–270
24. Vandevenne JE, Colpaert CG, De Schepper AM (1998) Subcutaneous granuloma annulare: MR imaging and literature review. Eur Radiol 8:1363–1365